Li, S., Moreno, M., Rosenau, M., Melnick, D., Oncken, O. (2014): Splay fault triggering by great subduction earthquakes inferred from finite element models. - *Geophysical Research Letters*, *41*, 2, p. 385-391.

DOI: http://doi.org/10.1002/2013GL058598

AGU PUBLICATIONS

Geophysical Research Letters

RESEARCH LETTER
10.1002/2013GL058598

Key Points:
- Splay fault triggering is simulated using FEM models with gravity
- Triggering mechanism is directly dependent on the depth of megathrust slip
- Study provides a useful tool for predicting the activation of secondary faults

Supporting Information:
- Readme
- Table S1
- Text S1
- Figures S1–S7

Correspondence to:
S. Li,
shaoyang.li@gfz-potsdam.de

Citation:
Li, S., M. Moreno, M. Rosenau, D. Melnick, and O. Oncken (2014), Splay fault triggering by great subduction earthquakes inferred from finite element models, *Geophys. Res. Lett.*, *41*, doi:10.1002/2013GL058598.

Received 5 NOV 2013
Accepted 9 JAN 2014
Accepted article online 13 JAN 2014

Splay fault triggering by great subduction earthquakes inferred from finite element models

Shaoyang Li[1], Marcos Moreno[1], Matthias Rosenau[1], Daniel Melnick[2], and Onno Oncken[1]

[1]German Research Centre for Geosciences, Helmholtz Centre Potsdam, Potsdam, Germany, [2]Institut für Erd- und Umweltwissenschaften, DFG-Leibniz Center for Surface Process and Climate Studies, Universität Potsdam, Potsdam, Germany

Abstract We have investigated the influence that megathrust earthquake slip has on the activation of splay faults using a 2-D finite element method (FEM), taking into account the effects of gravity and variations in the frictional strength properties of splay faults. We simulated both landward-dipping and seaward-dipping splay fault geometries, and imposed depth-variable slip distributions of subduction events. Our results indicate that the two types of splay fault exhibit a similar behavior, with variations in frictional properties along the faults affecting only the seismic magnitude. The triggering process is controlled by a critical depth. Megathrust slip concentrated at depths shallower than the critical depth will favor normal displacement, while megathrust slip concentrated at depths deeper than the critical depth is likely to result in reverse motion. Our results thus provide a useful tool for predicting the activation of secondary faults and may have direct implications for tsunami hazard research.

1. Introduction

Subduction zone splay faults, which branch upward from a plate boundary megathrust and may extend up to the sea floor, have been identified on seismic and bathymetric images from many subduction margins, for example, at Cascadia [*McCaffrey and Goldfinger*, 1995], south-central Chile [*Melnick et al*., 2006], Sumatra [*Singh et al*., 2011], and Nankai [*Park et al*., 2002]. Slip along splay faults may occur during great megathrust earthquakes as well as independently; they often have steep dips and are capable of producing large vertical seafloor displacements, posing a significant tsunami risk [e.g., *Wendt et al*., 2009].

Slip during a great megathrust earthquake can be partitioned between the subduction interface and splay faults, as noted from field observations of surface ruptures on land [*Melnick et al*., 2012b; *Plafker*, 1965], and inferred from modeling with the support of geophysical and historical data [e.g., *Cummins and Kaneda*, 2000; *Park et al*., 2002]. The pattern of slip partitioning between the megathrust and splay faults, and the parameters controlling the activation of slip in splay faults remain, however, only poorly understood. This is largely due to the scarcity of direct observations during earthquakes and the offshore location of most splay faults.

Because of the variations in interface properties of the seismogenic portion of a megathrust fault with depth, *Lay et al*. [2012] proposed a domain characterization of earthquake rupture distributions along dip. Shallow, intermediate, and deep megathrust earthquakes can therefore separately fill the long term slip deficit accumulated through locking of the plate interface. Our investigations have focused on how the spatiotemporal variability of megathrust slip triggers motion along splay faults. We used finite element method (FEM) models to quantitatively investigate the effect that slip along a megathrust has on frictional splay faults, and how it influences the amplitude and spatial distribution of seafloor deformation. We included two splay fault geometries constrained by the central [*Geersen et al*., 2011] and south-central Chile [*Melnick et al*., 2012a] subduction zones, which have landward and seaward dip directions, respectively. We used three typical depth-varying megathrust earthquake scenarios following the A-B-C zonation of *Lay et al*. [2012] to investigate the effects that changes in coseismic static stress resulting from such events can have on splay faults (Figure 1).

2. Methods

We used the PyLith FEM software [*Aagaard et al*., 2013] to kinematically model the response of splay faults to subduction earthquakes. We set up a 2-D elastic model that incorporated the curved geophysically constrained geometry of the south-central Chile subduction zone [*Tassara and Echaurren*, 2012], which may

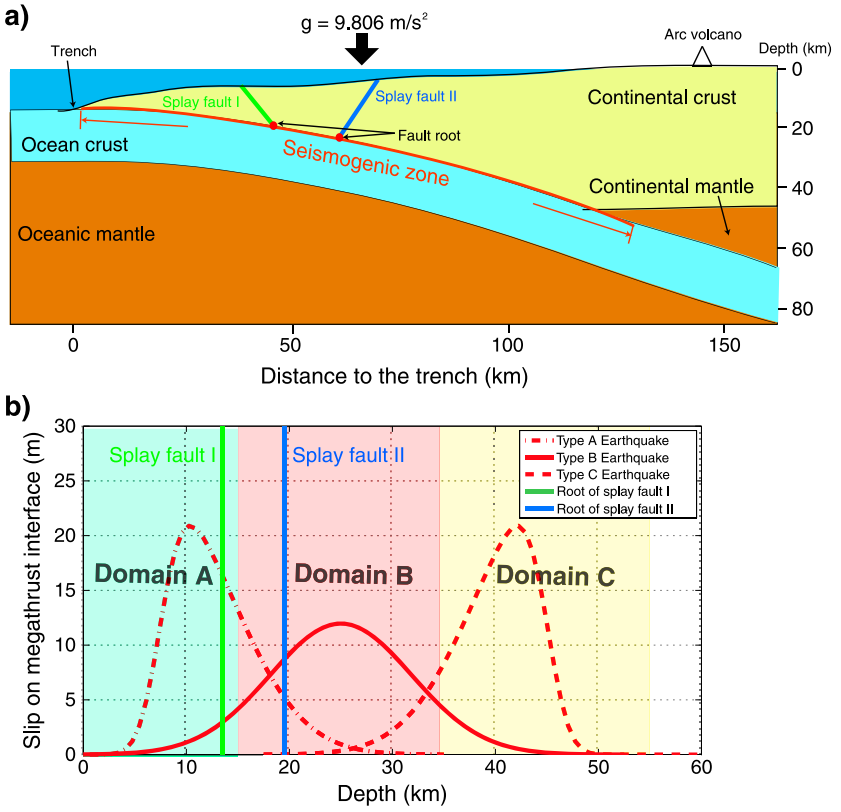

Figure 1. (a) Schematic plot of subduction zone. The seismogenic zone (red curve) is defined from the trench to the shallow intersection of the megathrust with the continental fore-arc Moho. Green and blue lines depict the dip directions of Type I and Type II splay faults, respectively. (b) Synthetic slip distributions of three characteristic earthquakes. The integral slips of the three earthquakes are all the same. The green and blue lines show the root zone depths of SF I and SF II, respectively, as shown in Figure 1a. Note that the megathrust earthquake in Domain A has a positive skew, so that part of the slip extends into both Domain B and Domain C; the earthquake in Domain B has a normal distribution with part of the slip extending into both Domain A and Domain C; the earthquake in Domain C has a negative skew and part of its slip extends into both Domain B and Domain C.

be considered representative of an accretionary margin, and two splay fault geometries (with landward and seaward dip directions) that mimic the major splay faults imaged from the central (SF I) [*Geersen et al.*, 2011] and south-central Chile (SF II) [*Melnick et al.*, 2012a] margins (Figure 1a), respectively. The latter was apparently triggered by the M_w 8.8 2010 Maule earthquake. SF I is equivalent to the megasplay fault found at the Nankai margin [*Baba et al.*, 2006]. The SF I splay fault has its root zone at 13.5 km depth and dips landward at an angle of 70°, while SF II has its root zone at 19.5 km and dips seaward at an angle of 60°. Both splay faults are rooted in the plate interface, with a distance of ~30 km between each other along the curved megathrust fault. In our investigations the section of the megathrust interface in which we allowed slip to occur extended from the trench down to shallow continental mantle at a depth of about 55 km (Figure 1a). The material properties used in the modeling are described on Table S1 in the supporting information.

We use three types of synthetic megathrust earthquake slip distributions (corresponding to the down-dip earthquake domains of *Lay et al.* [2012]) to systematically explore the responses of the splay faults to great subduction earthquakes (Figure 1b). The shallowest earthquakes (Type A) extend from the trench to about 15 km depth, the intermediate earthquakes (Type B) extend over a depth range of 15–35 km, and the deep earthquakes (Type C) extend from 35 to 55 km depth. We made synthetic slip distributions using a skew normal distribution [*O'Hagan and Leonard*, 1976] for Type A and Type C earthquakes and a normal distribution for Type B earthquakes (Figure 1b). We employed relatively high shape factors (see construction of skew normal distributions in the supporting information) for Type A and Type C earthquakes to mimic trench rupture earthquakes such as the 2011 Tohoku earthquake [*Ozawa et al.*, 2011; *Simons et al.*, 2011]. In our 2-D model we set the same amount of slip for all resulting earthquakes, i.e., identical seismic moments for the

three earthquake types. Note that we do not simulate earthquakes with slip in multiple domains. Detailed parameters for the characteristic slip distributions of the three types of earthquake are listed in Table S2.

Our modeling strategy consisted of three main steps for a complete kinematic scenario simulation. Steady state gravity stresses were first modeled on an extended model mesh without any megathrust or splay faults (Figure S1), using a high Poisson's ratio and quasi-rigid materials with a high Young's modulus $> 1.0 \times 10^{15}$ Pa [*Wang and He*, 1999] but keeping the same density as realistic materials. In this step no slip occurs on any faults and the resulting stresses were saved as the initial state. In the second step we released the gravity stresses (derived in the first step) along the splay faults in an additional simulation, by applying Coulomb's friction along these structures. If the initially derived gravity stresses were to be imported directly into the coseismic static stress calculation of the last step, these stresses would be released along the splay faults due to the sudden change in friction on the faults between the two steps of simulation, resulting in large displacements along these structures. In the third step the residual stresses from the second step were imported into a coseismic calculation with kinematic slip applied to the megathrust fault, using the same friction coefficient on the splay fault as was employed in the second step. Further explanation of the simulation strategy involving gravity and a sensitivity test of mesh size are presented in the supporting information. The material properties (Table S1) were kept constant for all kinematic simulations. With this multistage approach the boundary gravity stresses had no effect on near-field kinematic motion and the coseismic tectonic motion could be constrained by gravity stresses without producing any significant artifacts.

In order to investigate the responses of the splay faults to coseismic moment release, we varied the friction coefficient (μ) on the splay faults for each earthquake. In a preliminary test, we found large variations in splay fault slip when μ was between 0 and 0.1, and less variation when μ was greater than 0.1. We therefore carried out nonlinear sampling for different values of μ, i.e., 0.00, 0.01, 0.02, 0.04, 0.06, 0.08, 0.1, 0.2, 0.3, 0.4, 0.5, and 0.6 (Figure S2), for each megathrust earthquake simulation. We also varied the depth of the slip distribution for the three types of earthquake (A, B, and C) while keeping their slip distribution patterns stable, in order to investigate the spatial relationship between the position of the splay fault root zone and the megathrust earthquake centroid. To compare our results for SF I with those for SF II we adopted a parameter (H^*), this being the difference between the depth of the megathrust earthquake centroid (i.e., the mean slip location) and the depth of the splay fault root zone. In order to obtain uniform samples from the earthquake rupture centers within each of the A, B, and C domains, we explored slightly different sampling strategies for SF I and SF II with respect to the depths of their root zones (Table S3). In order to compare the splay fault mechanism, both quantitatively and qualitatively, we defined a rupture percentage parameter (R*) as the length of the fault rupture divided by the total length of the fault, with positive values representing normal faulting and negative values representing reverse faulting (Figure 3).

3. Results

Coseismic scenarios with no splay faults (i.e., with splay faults fully locked) were simulated with different types of megathrust earthquake, and used as references. As expected, the locus of maximum uplift and subsidence for Type A earthquakes shifts gradually landward for type B earthquakes, and again further landward for Type C (Figures 2a and 2b). We next explored the variations in splay fault slip between characteristic types of megathrust earthquakes (A-B-C zonation) using a range of splay fault friction coefficients (Figure S2 for SF I and SF II). The first-order sense of slip along the splay faults (i.e., normal or reverse) depended critically on the type of earthquake with shallow (e.g., Type A) earthquakes triggering normal slip on splay fault and deep (e.g., Type C) earthquakes triggering reverse slip (Figure 2 and Figures S4 and S5 in the supporting information).

We found that splay faulting locally modified the long wavelength coseismic surface deformation by adding a short wavelength but high-amplitude signal (colored curves in Figures 2a and 2b). In order to highlight the splay fault signal we calculated the vertical difference in surface displacement between simulations with frictional splay faults and the reference simulation with no splay faults (Figures 2c and 2d). For $\mu = 0$ on the splay fault, the splay fault induced vertical surface displacement shows a maximum perturbation (blue curve in Figures 2c and 2d). As μ on the splay faults is increased, the vertical surface displacements decrease until

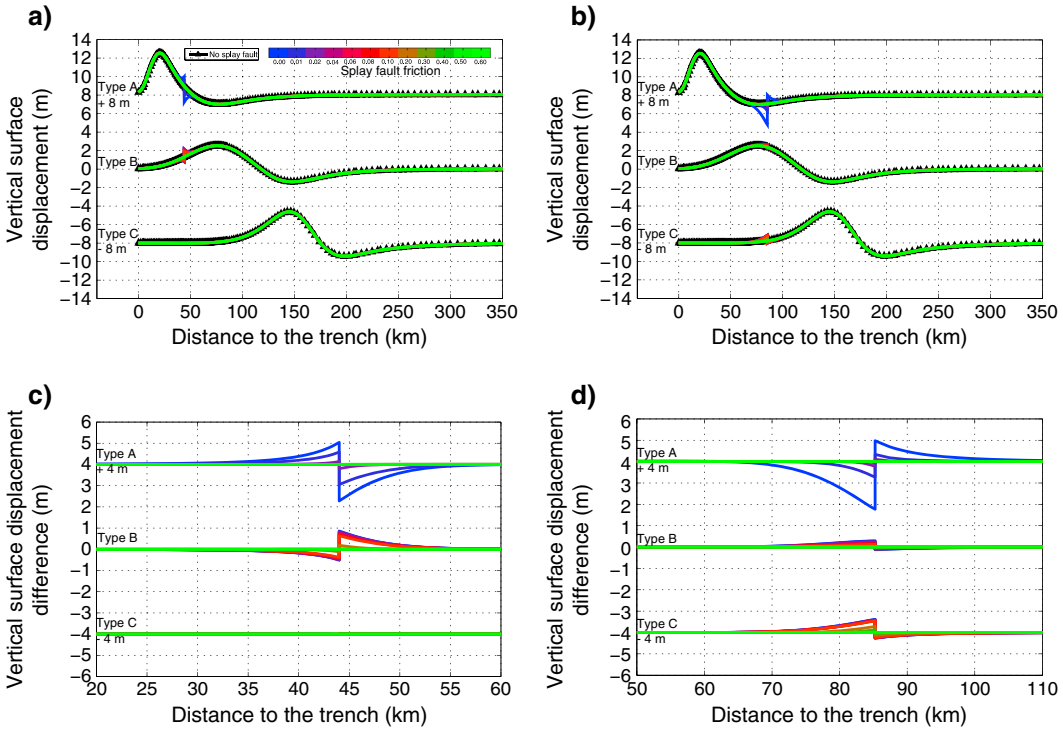

Figure 2. (a) Vertical surface displacement for three characteristic types of earthquake without a splay fault and with SF I with various coefficients of friction. From top to bottom, the megathrust earthquake ruptures mainly in the A, B, and C domains as characteristic A, B, and C type earthquakes, respectively. The black numbers within the panels (below the earthquake types) indicate the offsets of displacements in these plots. (b) Same as for Figure 2a but for SF II, with a similar legend. (c) Difference between the vertical surface displacement with and without SF I for the three characteristic megathrust earthquakes. The black numbers within the panels (below the earthquake types) indicate the offsets of displacements in these plots. (d) Same as for Figure 2c but using SF II instead of SF I. The legend is the same as for Figure 2c.

the splay faults become fully locked at $\mu = \sim 0.2$ (green curves in Figures 2 and S2, for SF I and SF II). The SF I splay fault shows an uplift of 1.1 m for the footwall together with a 1.9 m subsidence of the hanging wall (normal faulting) as a result of a typical Type A earthquake (blue curve, Figure 2c), i.e., a total of up to 4.0 m of local vertical seafloor displacement. For Type B and Type C earthquakes this displacement reduces to 1.5 m and 0.01 m, respectively, (blue curve, Figure 2c).

We then explored splay fault triggering in response to different earthquake depths. For each splay fault type (i.e. the 2 different types, as illustrated in Figure 1) and earthquake type (i.e. 9 different depth variations in total, as shown in Table S3) we simulated 12 different values of μ (as listed in Section **2**) on the splay fault. In total, therefore, we obtained 216 splay fault coseismic scenarios and 18 no-splay-fault references. We found that the splay faulting behavior was directly dependent on the megathrust earthquake centroid depth (Figure 3). With our model setting, we found a critical depth of megathrust centroid with respect to the splay fault root zone (H_c^*; Figure 3). Despite the different values μ of applied to the splay fault, the different splay fault dip directions and depths, and the different megathrust earthquake rupture patterns and depths, a megathrust rupture depth shallower than H_c^* resulted in normal faulting on the splay fault while a deeper megathrust rupture resulted in reverse faulting on the splay fault (Figure 3). Specifically, the SF I splay fault had a shallower critical depth than its root zone depth, which was located in the Domain A (Figure 3a), while the SF II splay fault had a critical depth deeper than the root zone, which was located in the Domain B (Figure 3b).

The plots of the difference between the megathrust earthquake centroid depth and the splay fault root zone depth (H^*) against μ for the two splay faults can be divided approximately into three regimes (by the solid pink lines in Figure 3). In Regime I the splay faults are fully locked and there is no splay fault activity triggered by megathrust earthquakes. In Regime II the splay faults are triggered as normal faults, and in Regime III the splay faults are triggered as reverse faults. The dashed purple lines in Regime II and Regime III indicate the conditions for full rupturing ($R^* = \pm 100\%$) of the splay fault.

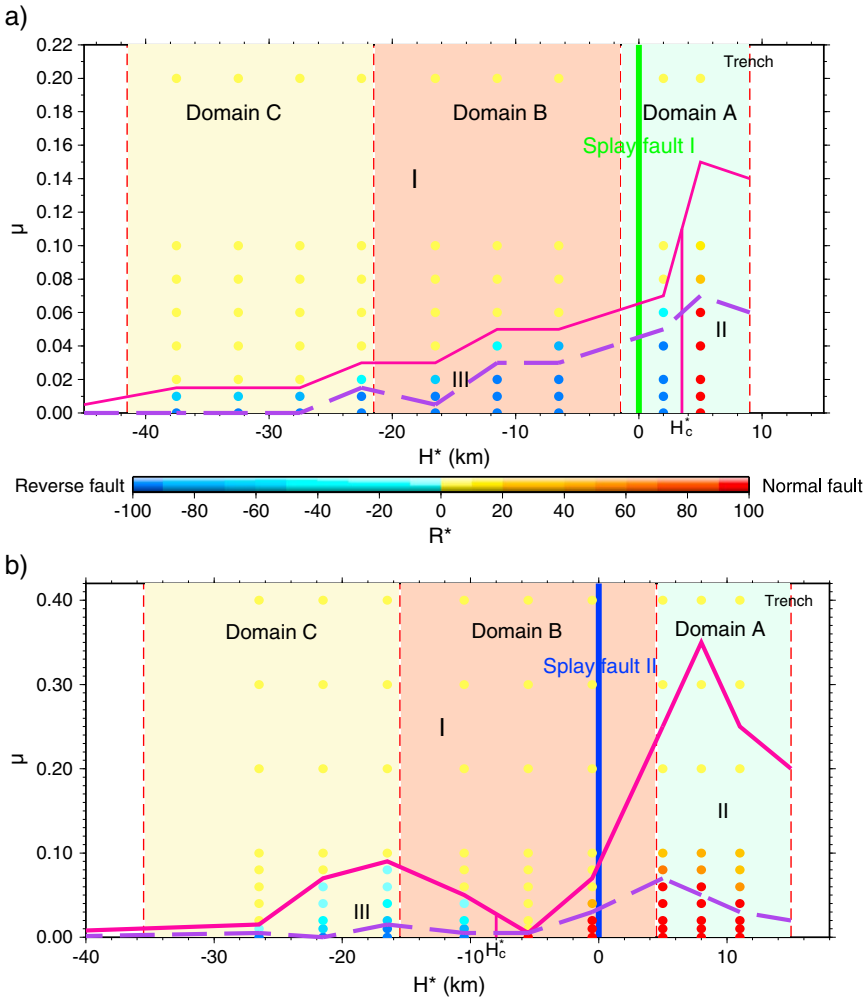

Figure 3. (a) Rupture behavior for SF I: relationship between the friction coefficient (μ) on SF I and the difference between the megathrust earthquake centroid depth and the SF I root zone depth (H^*). Bold green line indicates the position of SF I. (b) Rupture behavior for SF II: relationship between the friction coefficient (μ) on SF II and the difference between the megathrust earthquake centroid depth and the SF II root zone depth (H^*). Bold blue line indicates the position of SF II. The legend for Figure 3b is the same as for Figure 3a. Background colors indicate the megathrust earthquake domains of *Lay et al.* [2012]. The solid pink lines divide the whole coordinate space into Regime I, II, and III. The dashed purple lines in Regime II and Regime III indicate the boundaries for full and partial rupturing of the splay fault.

4. Discussion

Splay faults are weak zones in the overriding plate that can be repeatedly triggered by the static stress transfer from the great subduction earthquakes. Our results indicate that the splay fault can either fall into an area of increased Coulomb Stress Changes (CSC, positive and closer to failure) or an area of decreased CSC (negative and further away from failure) [*King et al.*, 1994; *Lin and Stein*, 2004] as the slip distribution moves along the megathrust interface. For example, Figure 3 shows that for a μ of 0.05 SF II can behave as locked, normal faulting or thrust faulting depending on H*. The results of CSC from characteristic Type A, B, and C earthquakes for both SF I and II are showed in Figure S6. Moreover, splay faults can be active as both normal and reverse faults during their lifetime, and can easily switch their mode depending on the critical depth H_c^* of megathrust centroid. Specifically, H_c^* is shallower than the root of SF I and deeper than the root of SF II. This means that even the centroid is a little shallower than the fault root of SF I, the deep slip (with respect to splay fault root) can overtake shallow part to trigger splay fault as reverse faulting; in contrast, the intersecting geometry of SF II and the megathrust fault favors normal motion. This observation is compatible with previous studies of dynamic modeling (e.g. [*DeDontney et al.*, 2012; *Kame et al.*, 2003]); due to the obtuse angle it is easier for slip propagation, although splay faults may be readily triggered by the dynamic rupture propagation in some cases. Therefore, the geometry of splay fault, especially the angle of splay fault to megathrust

fault, is likely to be an important factor in controlling H_c^*. Another controlling parameter could be inferred from our results is the slip pattern of megathrust earthquakes, because the shape of the slip function (i.e., skew normal or normal) strongly influences the centroid location.

Our modeling results are consistent with field observations during megathrust events. Triggering of reverse faulting in the outer fore arc (at the transition between Domains A and B) during the 1964 Alaska (M_w 9.2) [*Plafker*, 1965] and 2010 Maule (M_w 8.8) earthquakes [*Melnick et al*., 2012b] is consistent with the slip distribution during both events in Domain B. In turn, normal motion on inland splay faults (located above Domain C) occurred after the 2011 Tohoku, where slip mostly occurred in Domain A [*Asano et al*., 2011], and the northern segment of the 2010 Maule earthquake [*Ryder et al*., 2012]. Moreover, seafloor geodetic studies related with the 2011 Tohoku earthquake revealed significant horizontal displacement and uplift in the near and at the trench [*Kodaira et al*., 2012; *Tsuji et al*., 2013] indicating the activation of secondary structures, which are consistent with the results of our case of Type A megathrust earthquake with SF I (Figures 2c and S3c).

Our numerical experiments revealed constraints on the frictional properties of splay faults. We found that when the friction coefficient on a splay fault exceeded ~0.2 (i.e., Regime I in Figure 3), the splay fault was not triggered by any of the simulated megathrust earthquakes. This implies that splay faults in general need to be very weak (with about one third of the dry friction of rocks, according to *Byerlee* [1978]) to be triggered by megathrust earthquakes. Fault weakness could be due to high pore fluid pressure or to the presence of minerals with low friction coefficients (e.g., clay minerals) along the fault. Moreover, SF II has a relatively large friction window for splay fault activity compared to SF I (Figure 3). This implies that seaward-dipping splay faults like SF II are more susceptible to triggering than landward-dipping splay faults similar to SF I during megathrust earthquakes within a subduction zone.

If the friction coefficient on a splay fault varies with time causing a small reduction in the effective coefficient of friction (e.g., through fluid release), it can release compressive or extensional stresses induced by earlier megathrust faulting (with a certain time delay). This may explain some large aftershocks in the upper plate, such as that occurred 11 days after the 2010 Maule earthquake [*Ryder et al*., 2012] and 27 days after the 2011 Tohoku earthquake [*Asano et al*., 2011]. Furthermore, a megathrust earthquake rupture can trigger different fault behavior in different splay faults due to variations in their H_c^* values. This may explain the systematic variation of aftershock focal mechanisms within the forearc as a function of distance from the trench, which has been observed after great subduction earthquakes in Japan [*Asano et al*., 2011] and Chile [*Agurto et al*., 2012].

Our results show that seafloor/land surface deformation from movement along a splay fault is confined to the vicinity ($<$ 25 km) of the splay fault tip. The splay fault signal has one tenth of the wavelength and one half of the amplitude of warping from deep megathrust slip. When analyzing seismic hazards within a fore-arc zone the megathrust earthquake cycle should therefore receive priority consideration, and the splay (upper plate) fault earthquake cycle second-order consideration. However, splay faults can cause far greater surface deformation when triggered by Type A earthquakes than when triggered by deeper (Type B/Type C) earthquakes with the same moment. Even if deeper megathrust earthquakes trigger splay fault activities, the minor effects of such splay faulting are incapable of causing a large tsunami. Furthermore, we found that the location of the splay fault induced second-order signal that lay landward of the uplift peak for Type A events, and seaward of the uplift peak for Type B and Type C events. This means that the second-order signal for tsunamis triggered by Type A earthquakes would only be detectable (as a possible precursor wave to the main tsunami crest) in the near field. The signal would probably be undetectable in a tsunami wave field caused by Type B and Type C events because it would interfere with backwash in the near field and would be absorbed by the longer-wavelength waves during propagation to the far field.

5. Conclusion

Our results indicate that splay fault behavior depends on the relationship between the megathrust centroid depth and the critical depth: if the megathrust centroid depth is shallower than the critical depth, the splay fault may be triggered in normal slip; if the megathrust centroid depth is deeper than the critical depth, the splay fault may be triggered in reverse motion. The critical depth may be controlled by the splay fault geometry and the megathrust slip distribution pattern. Observation of coseismic splay fault behavior therefore offers another way of constraining megathrust coseismic rupture, in addition to the methods traditionally employed. Splay faults in the upper plate can have a local effect on the spatial distribution and magnitude of seafloor and land surface deformation. Our study has suggested a useful tool for predicting the activation of secondary faults that is not usually included in slip inversion methods and has implications for tsunami hazard research.

Acknowledgments

Shaoyang Li gratefully acknowledges the scholarship granted to him by the China Scholarships Council (201206040055). Marcos Moreno has been supported by the MARISCOS project MO 2310/1-1, and Daniel Melnick by grant ME 3157/2-2, both from the German Science Foundation (DFG). The authors would like to thank Brad Aagaard for his support with using the PyLith software. We also benefited from discussions with Jan Botle, Jonathan Bedford, and the members of the GeoSim graduate research school. Some of the figures in this paper were created with GMT software [*Wessel and Smith*, 1998].

The Editor thanks Christodoulos Kyriakopoulos and an anonymous reviewer for their assistance in evaluating this paper.

References

Aagaard, B. T., M. G. Knepley, and C. A. Williams (2013), A domain decomposition approach to implementing fault slip in finite-element models of quasi-static and dynamic crustal deformation, *J. Geophys. Res. Solid Earth*, *118*, 3059–3079, doi:10.1002/jgrb.50217.

Agurto, H., A. Rietbrock, I. Ryder, and M. Miller (2012), Seismic-afterslip characterization of the 2010 M_W 8.8 Maule, Chile, earthquake based on moment tensor inversion, *Geophys. Res. Lett.*, *39*, L20303, doi:10.1029/2012GL053434.

Asano, Y., T. Saito, Y. Ito, K. Shiomi, H. Hirose, T. Matsumoto, S. Aoi, S. Hori, and S. Sekiguchi (2011), *Spatial Distribution and Focal Mechanisms of Aftershocks of the 2011 off the Pacific Coast of Tohoku Earthquake*, pp. 5, Terra, Tokyo, Japan.

Baba, T., P. R. Cummins, T. Hori, and Y. Kaneda (2006), High precision slip distribution of the 1944 Tonankai earthquake inferred from tsunami waveforms: Possible slip on a splay fault, *Tectonophysics*, *426*(1–2), 119–134.

Byerlee, J. (1978), Friction of rocks, *Pure Appl. Geophys.*, *116*(4-5), 615–626.

Cummins, P. R., and Y. Kaneda (2000), Possible splay fault slip during the 1946 Nankai earthquake, *Geophys. Res. Lett.*, *27*(17), 2725–2728.

DeDontney, N., J. R. Rice, and R. Dmowska (2012), Finite element modeling of branched ruptures including off-fault plasticity, *Bull. Seismol. Soc. Am.*, *102*(2), 541–562.

Geersen, J., J. H. Behrmann, D. Völker, S. Krastel, C. R. Ranero, J. Diaz-Naveas, and W. Weinrebe (2011), Active tectonics of the South Chilean marine fore arc (35°S–40°S), *Tectonics*, *30*, TC3006, doi:10.1029/2010TC002777.

Kame, N., J. R. Rice, and R. Dmowska (2003), Effects of prestress state and rupture velocity on dynamic fault branching, *J. Geophys. Res.*, *108*(B5), 2265, doi:10.1029/2002JB002189.

King, G. C. P., R. C. Stein, and J. Lin (1994), Static stress change and the triggering of earthquakes, *Bull. Seismol. Soc. Am.*, *84*, 935–953.

Kodaira, S., T. No, Y. Nakamura, T. Fujiwara, Y. Kaiho, S. Miura, N. Takahashi, Y. Kaneda, and A. Taira (2012), Coseismic fault rupture at the trench axis during the 2011 Tohoku-oki earthquake, *Nat. Geosci.*, *5*(9), 646–650.

Lay, T., H. Kanamori, C. J. Ammon, K. D. Koper, A. R. Hutko, L. Ye, H. Yue, and T. M. Rushing (2012), Depth-varying rupture properties of subduction zone megathrust faults, *J. Geophys. Res.*, *117*, B04311, doi:10.1029/2011JB009133.

Lin, J., and R. S. Stein (2004), Stress triggering in thrust and subduction earthquakes and stress interaction between the southern San Andreas and nearby thrust and strike-slip faults, *J. Geophys. Res.*, *109*, B02303, doi:10.1029/2003JB002607.

McCaffrey, R., and C. Goldfinger (1995), Forearc deformation and great subduction earthquakes: Implications for cascadia offshore earthquake potential, *Science*, *267*(5199), 856–859.

Melnick, D., B. Bookhagen, H. P. Echtler, and M. R. Strecker (2006), Coastal deformation and great subduction earthquakes, Isla Santa María, Chile (37°S), *Geol. Soc. Am. Bull.*, *118*(11-12), 1463–1480.

Melnick, D., M. Cisternas, M. Moreno, and R. Norambuena (2012a), Estimating coseismic coastal uplift with an intertidal mussel: Calibration for the 2010 Maule Chile earthquake (Mw = 8.8), *Quat. Sci. Rev.*, *42*(0), 29-42.

Melnick, D., M. Moreno, M. Motagh, M. Cisternas, and R. L. Wesson (2012b), Splay fault slip during the Mw 8.8 2010 Maule Chile earthquake, *Geology*, *40*(3), 251–254.

O'Hagan, A., and T. Leonard (1976), Bayes estimation subject to uncertainty about parameter constraints, *Biometrika*, *63*(1), 201–203.

Ozawa, S., T. Nishimura, H. Suito, T. Kobayashi, M. Tobita, and T. Imakiire (2011), Coseismic and postseismic slip of the 2011 magnitude-9 Tohoku-Oki earthquake, *Nature*, *475*(7356), 373–376.

Park, J.-O., T. Tsuru, S. Kodaira, P. R. Cummins, and Y. Kaneda (2002), Splay fault branching along the Nankai subduction zone, *Science*, *297*(5584), 1157–1160.

Plafker, G. (1965), Tectonic deformation associated with the 1964 Alaskan earthquake, *Science*, *148*, 1675–1687.

Ryder, I., A. Rietbrock, K. Kelson, R. Bürgmann, M. Floyd, A. Socquet, C. Vigny, and D. Carrizo (2012), Large extensional aftershocks in the continental forearc triggered by the 2010 Maule earthquake, Chile, *Geophys. J. Int.*, *188*(3), 879–890.

Simons, M., et al. (2011), The 2011 magnitude 9.0 Tohoku-Oki Earthquake: Mosaicking the megathrust from seconds to centuries, *Science*, *332*(6036), 1421–1425.

Singh, S. C., N. D. Hananto, and A. P. S. Chauhan (2011), Enhanced reflectivity of backthrusts in the recent great Sumatran earthquake rupture zones, *Geophys. Res. Lett.*, *38*, L04302, doi:10.1029/2010GL046227.

Tassara, A., and A. Echaurren (2012), Anatomy of the Andean subduction zone: Three-dimensional density model upgraded and compared against global-scale models, *Geophys. J. Int.*, *189*(1), 161–168.

Tsuji, T., K. Kawamura, T. Kanamatsu, T. Kasaya, K. Fujikura, Y. Ito, T. Tsuru, and M. Kinoshita (2013), Extension of continental crust by anelastic deformation during the 2011 Tohoku-oki earthquake: The role of extensional faulting in the generation of a great tsunami, *Earth Planet. Sci. Lett.*, *364*(0), 44-58.

Wang, K. L., and J. H. He (1999), Mechanics of low-stress forearcs: Nankai and Cascadia, *J. Geophys. Res.*, *104*(B7), 15,191–15,205.

Wendt, J., D. D. Oglesby, and E. L. Geist (2009), Tsunamis and splay fault dynamics, *Geophys. Res. Lett.*, *36*, L15303, doi:10.1029/2009GL038295.

Wessel, P., and W. H. F. Smith (1998), New, improved version of the Generic Mapping Tools released, *EOS Trans. AGU*, *79*, 579.